Effect of surface decoration on properties

and drug release ability of nanogels

Filippo Pinelli [a], Fabio Pizzetti [a], Arianna Rossetti [a], Zbyšek Posel [b,c],

Maurizio Masi [a], Alessandro Sacchetti [a], Paola Posocco [b,*], Filippo Rossi [a,*]

[a] *Department of Chemistry, Materials and Chemical Engineering "Giulio Natta", Politecnico di Milano, via Mancinelli 7, 20131, Milan, Italy*

[b] *Department of Engineering and Architecture, University of Trieste, via Valerio 6/A, 34127, Trieste, Italy*

[c] *Department of Informatics, Faculty of Science, Jan Evangelista Purkyně University, České Mládeže 8, 400 96 Ústí nad Labem, Czech Republic*

* Corresponding authors

E-mail address: paola.posocco@units.it

E-mail address: filippo.rossi@polimi.it

1

Abstract

Nanogels are a central class of biomaterials widely used in the field of drug delivery for the treatment of different pathologies such as tumors, cardiovascular diseases or central nervous system disorders. The great peculiarity of these systems is that, if properly surface functionalized, they are able to target specific body tissues and exploit precise targeted drug delivery. Anyway, the presence of a surface layer on the nanoparticle core can affect not only the biological behavior of the whole system but also its physical and drug delivery properties. In this work we investigated how the presence of different surface functionalization strategies on the same PEG-PEI nanogel framework influences the aforementioned peculiarities. The nanogels were functionalized with amine and pyridinic groups, while the properties analyzed and compared were the hydrodynamic diameter, the ζ-potential and the drug release ability. Moreover, we performed the evaluation of the cytocompatibility of the final nano-carrier and a molecular analysis of the surface features of these systems at microscopic level.

1. Introduction

Nano-systems are becoming very attractive materials in many biomedical applications such as drug delivery, tissue engineering or nanodiagnostics [1–3]. Widespread attention has been paid to targeted drug/gene delivery systems that allow the distribution of their cargos to target sites, increasing the therapeutic efficiency [4,5]. Indeed, these devices allow to localize drug effect, limit their side effects due to their lack of interaction with other tissues of the body, protect the drug *in vivo* from degradation and minimize symptoms and degenerative effects of diseases such as cancer, neurological injuries or cardiovascular diseases [6,7]. Commonly, targeted drug delivery is divided into either "passive" or "active" [8]. Passive drug delivery is based on the differences between normal areas and diseased tissues that determine the accumulation of the carrier in the altered zone and it relies on the different distribution of the drug by blood circulation. Active drug delivery is instead a method aiming to reach a specific biological target, for example thanks to the conjugation of the delivery system with a certain ligand, such as an antibody, specific for a receptor on the surface of a peculiar cell population [9].

Literature presents a wide variety of nanocarriers and especially nanoparticles are able to meet the requirements about targeted delivery, modulation of cell response and controlled release of the cargo [10,11]. Among them, nanogels (NGs) are a very interesting class of nanobiomaterials [12,13]. Their formulation is compatible with biological tissues, due to a high water content and a peculiar carbon-based composition, which impart them biocompatibility and biodegradability. Moreover, NGs have high specific surface, excellent drug encapsulation ability and significant swelling behaviour with a remarkable structure stability and fast response to environmental changes that makes them extremely suitable for the selective target delivery [14,15].

Because of all the aforementioned peculiarities, NGs can be a pivotal device to target cells and treat them with proper drugs and active substances, but the possibility to obtain a selective and effective targeting still remain a big challenge hampered by the high selectivity of absorption of many cellular populations and the multiple membrane barriers to be overcome [16,17].

In order to satisfy these requirements, nanogels surface functionalization may become a strategic tool to impose to the nanosystem specific properties and so tuning its behaviour overcoming biological limitations and unwanted effects [18,19]. Responsive chemical groups or specific molecules can be chemically or physically linked to the NG structure to promote specific interactions with cells receptors and to trigger the endocytosis of the nanocarrier inside the cytosol of the cells [20–23] In fact, there are many examples in literature about how the presence of layers of different nature on a specific core is able to modify the properties of the entire system [24–27].

We have already investigated this aspect in previous works [11,28,29]; nonetheless, since the NGs behaviour in vivo is influenced by the surface physical-chemical properties [30], in this work we are interested in studying how the moieties used to modify the NGs surfaces affect the physical properties of the system and in particular the drug release ability, using rhodamine B (RhB) as a model drug. The NGs tested for our purpose were synthetized with polyethylene glycol (PEG) and linear polyethyleneimine (PEI) and conjugated with a chromophore in order to ensure *in vitro* detection. The decorative functionalization strategies were realized using two different molecules: the 3-bromopropylamine hydrobromide and the 4-(bromoethyl)pyridine hydrobromide, selected in order to analyze the effect of the presence of an amine functionalization on the surface, in an aliphatic and aromatic form, respectively. Mesoscale simulations of each NG were carried out and established a link between NG properties and microscopic surface features.

2. Materials and Methods

2.1 Materials

Polymers: linear polyethyleneimine 2500 (M_w=2.5 kDa, by Polysciences Inc., Warrington, USA) and polyethylene glycol 8000 (M_w=8 kDa, by Merck KGaA, Darmstadt, Germany). All other chemicals where purchased from Merck (Merck KGaA, Darmstadt, Germany) and used as received, without any further purification. Solvents were of analytical-grade purity. All the rhodamine-based products were stored at 4°C.

2.2 Characterization techniques

Fourier transform infrared (FT-IR) spectra were recorded using the KBr pellet technique for the analysed samples and a Thermo Nexus 6700 spectrometer couplet to a Thermo Nicolet Continuum microscope equipped with a 15 x Reflachromat Cassegrain objective at room temperature in air in the wavenumber range 4000-500 cm^{-1}, with 64 accumulated scans and at a resolution of 4 cm^{-1}. The size, polydispersity index (PDI) and ζ-potential of nanogels were investigated using the Dynamic Light Scattering (DLS) technique while morphological evaluation with Atomic Force Microscopy (AFM) analysis as discussed in previous work [28, 29]

2.3 Nanogel synthesis

The nanogel synthesis was performed as described in details in our previous works [29,31]. Briefly, in the first step of the preparation the PEG hydroxyl group was modified using carbonyldiimidazole (PEG-CDI), while propargyl-PEI was functionalized with rhodamine B azide using the copper-catalyzed azide-alkyne Huisgen cycloaddition (CuAAC) reaction. Then two solutions were prepared: in the first one the functionalized PEG (200 mg, 0.025 mmol) was dissolved in CH$_2$Cl$_2$ (3mL), while in the second solution the PEI conjugated with RhB (52 mg, 0.017 mmol) was dissolved in distilled water (5 mL). The organic solution was added dropwise to the aqueous one under stirring at r.t. and the final system sonicated for 30 minutes.

Then the mixture was allowed to stir for 17 hours at room temperature (25°C) promoting the evaporation of CH_2Cl_2. Finally, the obtained aqueous solution was purified through dialysis against slight acid water (M_w cut-off = 3.5 kDa) and lyophilized. These nanogels were used as a reference for cell internalization and they were labeled as NGs.

2.4 Nanogel decoartion with -NH₂

The primary amine grafting around the nanogel surface was performed as discussed in our previous work [29]. Briefly, NGs (15 mg) were dissolved in distilled water (1 mL) and the 3-bromopropylamine hydrobromide (4.95 mg, 22.64 μmol) was dissolved in distilled water (0.5 mL) and added dropwise to the nanogel solution. The mixture was stirred for 17 hours and successively the solution was dialyzed (M_w cut-off = 6-8 kDa) against distilled water for 3 days, with daily water exchange, allowing the removal of unreacted species. The system was frozen at -80°C and the product was finally recovered through lyophilization. This typology of coated nanogels will be indicated with NG-am.

2.5 Nanogel decoration with pyridinic group

The pyridinic group was grafted to the surface of reference nanogel with a procedure similar to the one previously explained. NG-ref (15 mg) were dissolved in distilled water (1 mL) while 4-(bromoethyl)pyridine hydrobromide (10 mg, 40 μmol) was dissolved in another vial of distilled water (1 mL). This latter solution was added dropwise to the nanogels' solution under stirring at room temperature (25°C) and the system was left under stirring for 17 hours. The final solution was dialyzed (M_w cut-off=6-8 kDa) against distilled water (1 L) for 3 days, with daily water exchange, allowing the removal of unreacted species. The system was frozen at -80°C and the product was finally recovered through lyophilization. These nanogels from now on will be indicated with NG-pyr.

2.6 Loading of nanogels with rhodamine B and in vitro drug delivery

The nanogels were loaded with rhodamine B, commonly used in literature as drug mimetic [32,33]. To optimize drug loading in previous work we studied two different strategies. In the first, the drug was entrapped in the swollen preformed NG as follows: a polytetrafluoroethylene (PTFE) cylinder 1 cm in diameter and 1 cm long with an axial perforation of 1 mm diameter and a radial one of 500 μm was used for mixing (Figure SI5 a). The NG water suspension (1 mg/mL) and the dissolved Rolipram drug solution in ethanol (0.014 mg/mL) were loaded in syringe pumps and injected radially into the device at a flow rate of 1 mL/min. For the second procedure lyophilized NG was suspended directly in drug solution and mixed until dissolution. The swelling NG establishes high concentration gradient between the solution and the inner core of the NG (Figure SI5 b). Then, loaded NG was dialyzed (membrane Mw cutoff = 3500 Da) against aqueous solution for 30 min in order to remove free drug molecules. The results obtained were similar and in this work we decided to use the second one. Drug release mechanism was investigated at pH 7.4 using a phosphate buffered saline solution (PBS). In details, each loaded nanogel sample was placed, within a dialysis bag (cut-off=1500 Da), in excess of PBS and aliquots (3×100 μl) were collected at defined time points, while the sample volume was replaced by fresh solution, in order to avoid mass-transfer equilibrium with the surrounding release environment. The experiments were performed at 37 °C. Percentages of released RhB were then measured by UV spectroscopy at a specific wavelength ($\lambda = 570$ nm). Loading efficiency (% loading) was calculated referring to the equation:

$$\% \, loading = \frac{initial \, amount \, loaded - free \, drug}{initial \, amount \, loaded} \cdot 100 \qquad (1)$$

Drug diffusion mechanism can be described as 1-dimensional model of the second Fick law as discussed in previous work [28, 34] where the nanogel geometry is a sphere and the material flux mainly takes place at the nanogel/PBS surface.

2.7 Cytocompatibility evaluation of nanogels

Mouse fibroblasts (L929) were cultured in complete medium (Dulbecco' s modified Eagle's medium (DMEM) supplemented with 10% fetal bovine serum, 1% penicillin/streptomycin, 1% L-glutamine 200 mM. L929 were seeded in 24-well plates at concentration of 50,000 cells/well in 1 mL complete medium and grown at 37 °C, 5% CO_2. After 24 h, the medium was changed and NGs (0.05% weight/volume) were then added to cell cultures for up to 3 days. After 3 days of culturing, the cytotoxicity of macrostructure was evaluated by performing an MTS assay.

The absorbance was measured at 570 nm, and the results were compared with that of the control wells to determine relative cell viability.

2.8 Molecular modeling of NG surfaces

Coarse-grained (CG) representation of each NG surface was performed and we retrieved the surface behavior by means of dissipative particle dynamics (DPD) [35] [36–38]. DPD has been already successfully used in the prediction scale and phase behavior of polymer brushes and solvent-responsive brushes in smart nanofluidic devices [39–41]. Thanks to the short length of the coating groups we adopted a simplified model of the surface as a flat PEG-PEI plane to which the functional layer is linked. The system is represented by DPD segments (also called *beads*), at CG level, and contains several atoms depending on the CG level where one bead represents one water molecule. The surface of the nanogel was modeled as a collection of PEG-PEI beads kept frozen, i.e. not moving throughout the simulation. The decaorative layer was then built as an ensemble of bead-spring chains randomly attached at a density of 1.2 and 2.4 chains/nm^2 for NG-am and NG-pyr, respectively, based on a putative estimation from experimental functionalization data. Full details of the CG models can be found in the SI. The DPD bead interaction parameters were evaluated using the solubility parameters estimated by Hansen theory [42] and mapped into the Flory-Huggins parameter [43]; electrostatic interactions were modeled by replacing point charges with Gaussian distributions [44,45].

Standard Ewald summation was used to evaluate interaction of charged beads with the real-space cutoff set to zero and the homogeneous relative dielectric constant to $\varepsilon_r = 80$. All simulations were carried out in LAMMPS [46] and trajectories analyzed by in-house developed code. Visualization was done in VMD tool. More simulation details are provided in the SI.

2.9 Statistical analysis

Where applicable, experimental data were analyzed using Analysis of Variance (ANOVA). Statistical significance was set to p value < 0.05. Results are presented as mean value ± standard deviation.

3. Results and discussion

3.1 Nanogel chemical characterization

The nanogel synthesis was performed with the reaction between the bis-functionalized PEG-CDI and the rhodamine-PEI through the emulsification evaporation method (Figure 1A). After sonication, the progressive evaporation of CH_2Cl_2 from the emulsion encourages the homogeneous dispersion of PEG chains around PEI. This conformation is a pivotal condition in order to meet the biocompatibility criteria with the cellular environment. In fact, PEI has shown toxic effects on cells especially when used alone[47]: the grafting and mixing with PEG that is a non-toxic and non-immunogenic polymer guarantees to the final system a high degree of solubility in water and great biocompatibility of the entire system[48]. In this work, we have functionalized PEG with an excess of CDI to trigger the bis-functionalization of the polymer. On the other hand, the functionalization of PEI with RhB involves on purpose a small portion of amine groups of the polymer, preserving most of them for the reaction with CDI-PEG, as widely discussed in our previous works [29,49]. The synthesized nanogels (here NG-ref) were characterized through FT-IR analysis and the results, showed in the Figure 1B, confirm the occurred synthesis [29]. The carbamate group (as shown in Figure 1A) could be recognized at 1620 cm^{-1} (**1**, asymmetric stretching COO$^-$), 1440 cm^{-1} (**2**, symmetric stretching COO$^-$) and 1290 cm^{-1} (**3**, N-COO$^-$ stretch). The synthesis allows us to obtain monodispersed gel particles with small and controllable size as visible from DLS analysis (Figure1C).
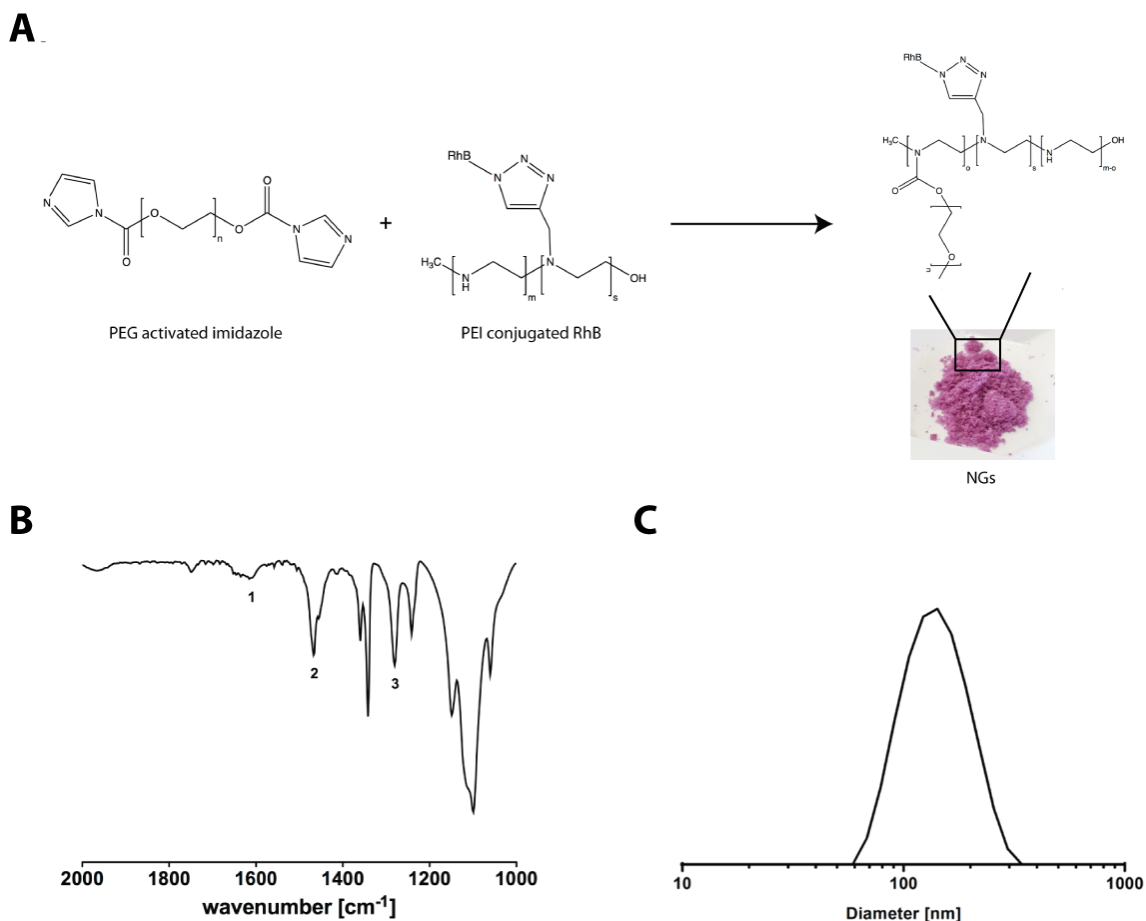
Figure 1. (A) Scheme of nanogel synthesis and resulting putative structures of NGs; (B) FT-IR characterization of NGs; (C) DLS measurement of NGs.

3.2 Nanogel decoration strategies

As aforementioned, two main strategies for rhodamine labelled nanogels were studied. First, we evaluated the effect of amine group covering the nanogels surface using 3-bromopropylamine hydrobromide: in this case the 3-bromopropylamine nucleophilic substitution involved the residual PEI amine groups without affecting the nanogels bonds and preserving the framework of the polymeric system. Then the functionalization with the pyridinic group was performed in a similar way using 4-(bromoethyl)pyridine and also in this case the nucleophilic attack takes place from the free -NH sites present in the PEI molecules of the NG-ref structure.

In all cases, the molecules used to perform the functionalization were used in large excess with respect to the NG-ref molecules in order to trigger the functionalization. In Figure 2 the schematization of these functionalization strategies on NGs -NH free sites is reported and act as anchoring groups (FT-IR spectra in SI).
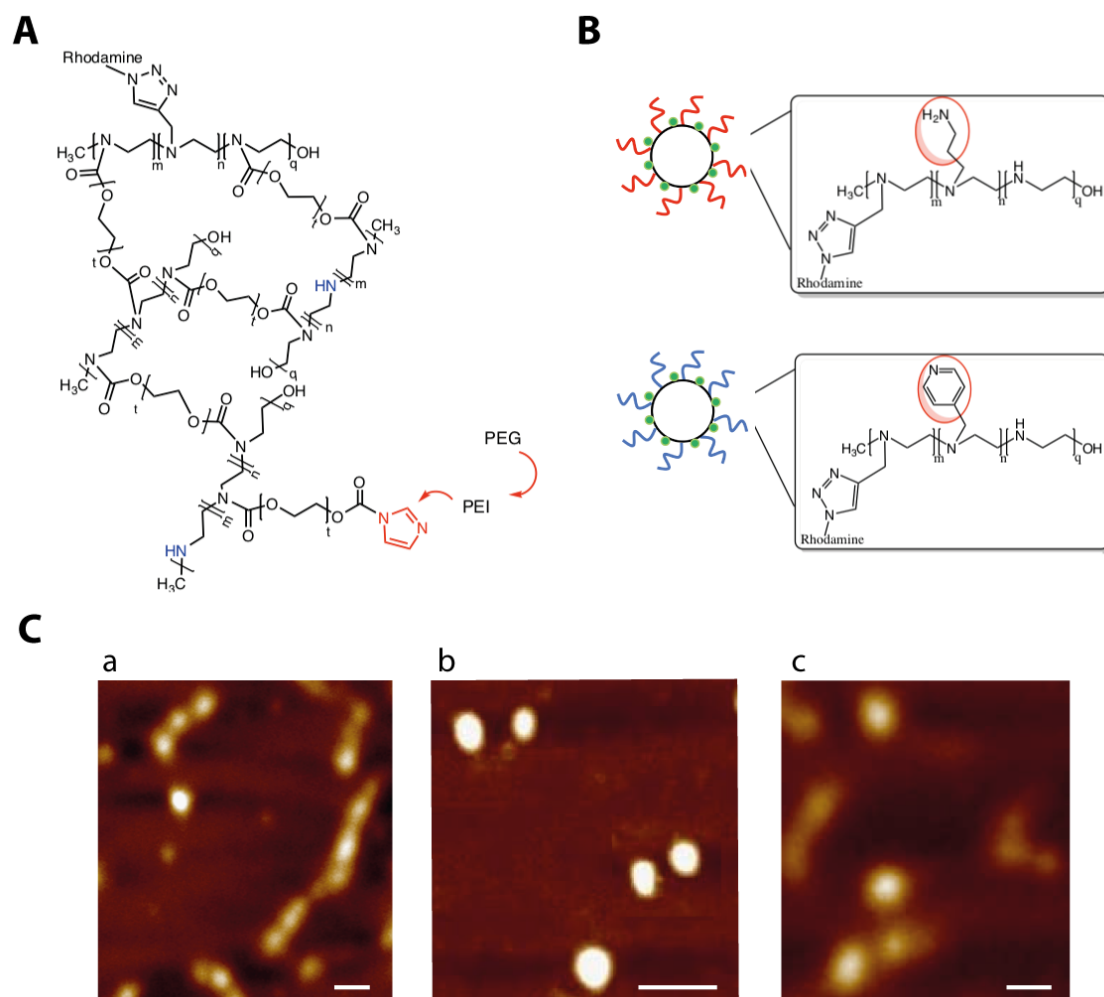

Figure 2. (A) Schematization of the cross-linking process between PEG and PEI to form the NG framework; (B) focus on the functionalization of the external PEI chains with different molecules in NGs framework; (C) AFM images of fluorescent coated nanogels: NG-ref (a), NG-am (b) and NG-pyr (c) from left to right. Scale bars: 300 nm.

The effects of decoration on the nanogel structure and physical properties of the system were then investigated using the DLS technique, since the hydrodynamic diameter could be affected by solvation or protonation effects on the nanogel surface.

At the same time, it is interesting to study the impact on the ζ-potential of the different chemical groups used to functionalize the surface. The obtained results are reported in Table 1. All the samples were characterized by hydrodynamic diameter values between 155 and 223 nm, that enable potential cellular internalization: in details, NG-am were smaller, while NG-pyr larger than uncoated NGs and their interaction with living cells could be strongly influenced by these small differences. This size variation is mainly related to the grafting of the new functional groups on the nanogel surface. In fact, despite their presence increases the steric hindrance of the systems and could determine a prominence of the swelling behavior, important changes can be also observed in the ζ-potential of the functionalized nanogel. The distributed charge can be strongly affected by the presence on the surface of the nanogel of diverse chemical groups [30]. As mentioned in our previous work [29] the presence of primary -NH$_2$ surface groups determines nanogel protonation and a positive charged interface. This phenomenon is not observed in the case of decoration with the pyridinic group, when the ζ-potential values maintain an almost neutral value. Moreover, it can be noticed that NG-am and NG-pyr present similar values of PDI higher than NG-ref: this increase can be explained due to the presence of an additional steric hindrance present on the nanogel surface.

Table 1. Nanogel DLS (mean values, n = 3) measurements in PBS.

Nanogel type	Diameter [nm]	PDI [-]	ζ-potential [mV]
NG-ref	190	0.15	0.01
NG-am	155	0.2	3.05
NG-pyr	223	0.21	-0.096

Morphological evaluation can be observable from AFM analysis (Figure 2): all particles showed a spherical and smooth surface with sizes similar and partially comparable with the ones obtained with DLS. The slight variations are relative to the sample processing between DLS and AFM analyses that is different.

Indeed, while DLS analysis is performed in aqueous solutions (measures hydrodynamic radius) AFM, measurement is conducted in dry state. Due to this fact it is not possible to observe with AFM the same differences, in term of diameter, visible with DLS. In Figure 3 the evolution of the particle size versus time is reported and it is possible to observe that, in all cases, the NGs diameter remains substantially unaltered; in fact, only minor changes are visible underling the colloidal stability and absence of aggregation (same results were collected also in cell culture medium present in Supporting Information). The same trend is observable also for coated NGs, finally proving the efficiency and stability of the added coating strategies.
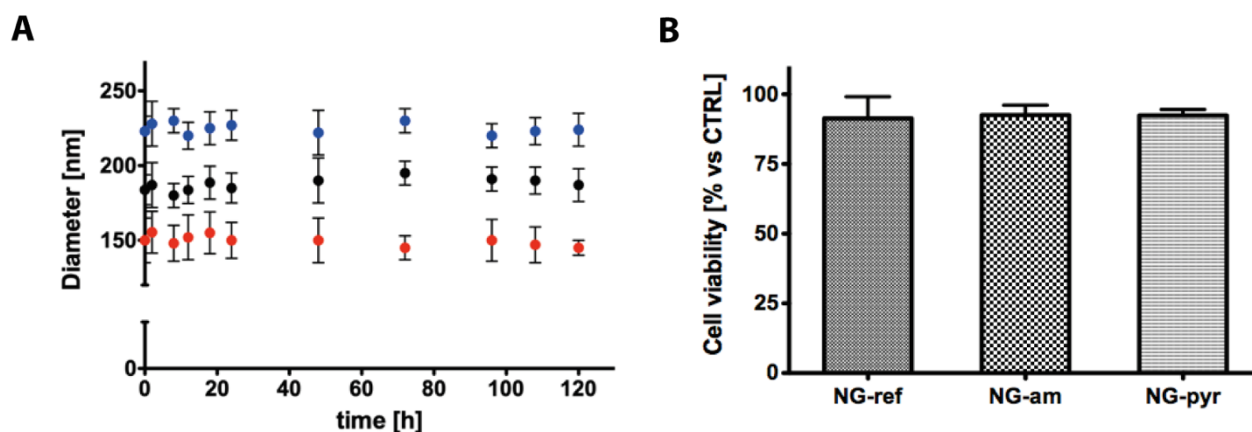
A

B

Figure 3. A) Particle size (n = 3) versus time of NG-ref (black circles), NG-am (red circles) and NG-pyr (blue circles). (B) Fibroblast viability after incubation for 3 days in the presence of nanogels. The columns represent the mean ± S.D.; n = 3.

Cytocompatibility of nanogels (NG-ref, NG-am and NG-pyr) was evaluated in vitro culturing L929 fibroblasts for 3 days then measured with MTS assay. The concentration of NGs used is the same used in pharmacological treatments and in other biomedical studies [48]. The results, in Figure 3, clearly showed the absence of potentially toxic components in all the NGs tested respect to control group (100% in the graph).

3.3 Mesoscopic simulation of the nanogel surfaces

In our previous work [29] we carried out a study focused on molecular aspects of nanogel surfaces functionalized with specific moieties. At that time, we analyzed NG-am, highlighting its peculiarities and behavior in aqueous environment. We decided to reproduce that analysis in this work to unfold other families of modified nanogels following the same guideline, which has been proven accurate in studying coating and chain packaging at nanoscale. Modification of nanogel surface with anchoring molecules or functional groups is expected to alter the nature of the surface with a layer of just a few nanometers thick. Depending on the number of tethering points and chemical structure of the decoration layer, the effects can be confined – generating surface anisotropy – or extended over the entire surface. Thus, it is essential to know how the coating shell behaves either in terms of arrangement of grafted groups and local distribution of the solvent to unveil the length scale of functionalization, surface homogeneity and topography.

A molecular snapshot of NG-am and NG-pyr surface is reported in Figure 4. Visual inspection of the systems as predicted by DPD calculations reveals that NG-am and NG-pyr achieved a different level of coverage, which reflects in dissimilar local arrangement of anchored chains and water molecules. Two-dimensional density maps of system components were then derived, averaging over the PEG-PEI surface and the molecular height of the functional layer (known as "brush height" [40]). This provided us with quantitative information about chain organization and how the PEG-PEI surface is shielded from the external solvation environment at microscale (Figure 4). NG-am and NG-pyr nanogel are endowed with a different degree of hydration, being the latter described by a less solvated microenvironment (Figure 4A and B). To compare the content of solvent within the layers with that of unmodified NG, values were normalized to the average water density in NG-ref. In both cases, we observed a lower local water content in the functionalized surfaces. Water distribution appeared more homogenous in NG-pyr caused by the higher density of tethered chains, while the less extent of functionalization in NG-am induced areas of discontinuous water concentration.
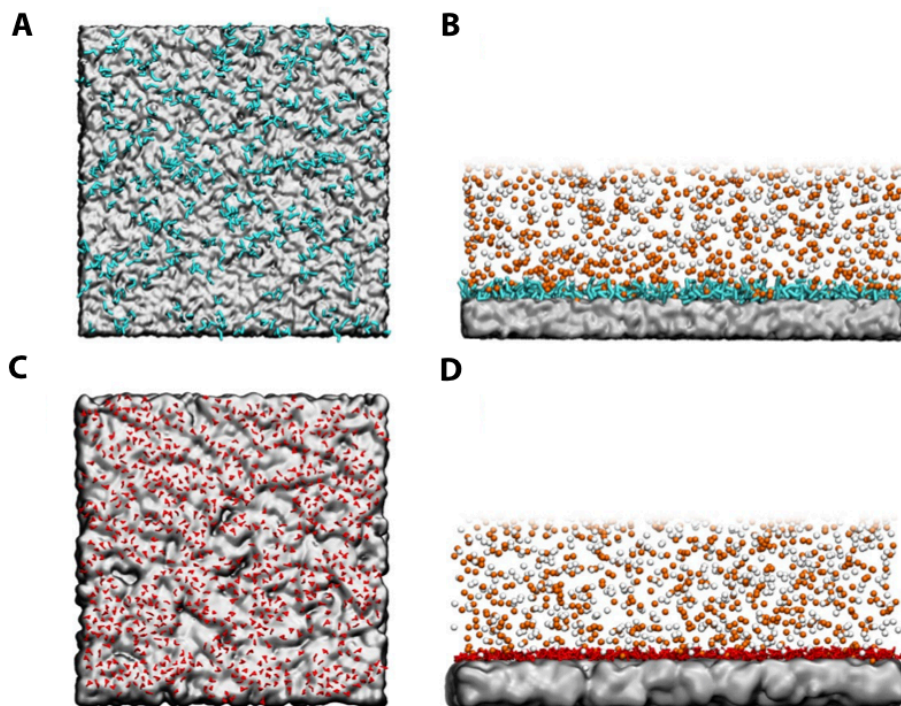
Figure 4. Top- and front-view snapshots taken from equilibrated surface structure of NG-am (A-B) and NG-pyr (C-D). Sodium and chlorine beads are depicted as white and orange spheres, respectively. Water is not shown for clarity.

Density maps of chain distribution are then reported in Figure 5, with values normalized to the average polymer concentration in each system to allow quantitative comparison between the surfaces. Red (to green) areas thus represents zones where the concentration of grafted moieties is higher, while blue patches indicate parts of the surface where solvent prevails. Having this in mind, we saw that NG-am presents large unfunctionalized areas exposed to water molecules, which resemble NG-ref surface. Conversely, in NG-pyr the functional groups are less localized and areas where chains are absent are smaller in size and more uniformly distributed over the layer.
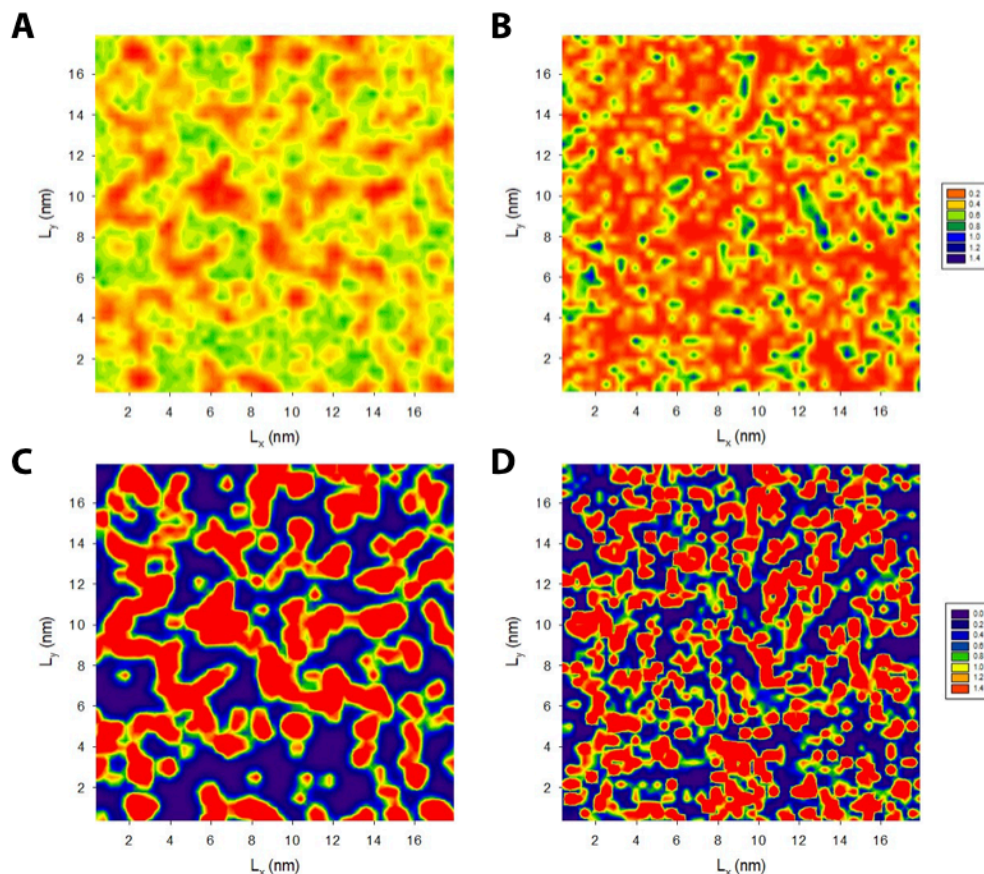
Figure 5. Two-dimensional density maps of solvent (A and B) and tethered chains (C and D) for NG-am (A-C) and NG-pyr (B-D) system. Water density values are scaled to the average water content in NG-ref, while chains per unit area are normalized by the average chain value in the corresponding system.

3.4 Drug release profiles

Once proved that PEG-PEI colloidal gel systems were successfully functionalized with different chemical groups, their role in drug release was studied using RhB as a drug mimetic. The results collected were compared with the case of neat NGs already published (black circle, Figure 6) [50]. This study is necessary to investigate the benefits related to the use of different decoration strategies in our nanogel system. Release studies were conducted at 37 °C at pH 7.4. RhB was chosen for this investigation because its steric hindrance and its functional chemical groups resemble many drugs containing free carboxylic acid or carbonyl group, commonly used in pharmaco-therapy, for example, to treat CNS damages or cancer side effects [51–54].

The values of loading in the different typologies of NGs confirm an efficient encapsulation in the NGs framework and are listed in Table 2. As known in literature, colloidal nanoparticles present the ability to load and carry drugs with three main mechanisms: loading them within their core, adsorbing them in their external layer (coating) and coordinating them with electrostatic interactions [55,56]. We investigated the last one in previous study [57]; in this work we are interested in understanding the role of adsorption that generally is underestimated. Being the nature of the inner part the same for these three colloids, the ability to load drugs within them is the same [33] and so we focused our attention on the two other mechanisms involved. From Table 2 it is visible that coated NGs are able to load higher percentage of drug with respect to uncoated NGs. The increasing of adsorbing sites in outer layer causes higher loading ability and so, not only drug entrapment but also drug adsorption is very important, underlining that decoration of NGs is a promising strategy to increase drug loading.

Table 2. Loading percentages of RhB for NGs, NG-am and NG-pyr.

Nanogel type	Percentage of loading
NG-ref	60%
NG-am	85.3%
NG-pyr	81.4%

The percentage of RhB released (Figure 6) was defined as the ratio between the released amount in the aqueous media and the total amount loaded into the NGs. In Figure 6 the release profiles of RhB, investigated after incubating the samples at 37°C in PBS, are presented as ratio between the released amount in PBS and the amount effectively loaded within NGs with different decoration strategies then compared with neat ones. In Figure 6A release profiles from NG-ref (black), NG-am (red) and NG-pyr (blue) are visible and in Figure 6B zoomed in the first 24 hours. In all cases RhB release presented a biphasic pattern with an initial burst release followed then by a sustained release prolonged in time until 15 days.

The coated NGs presented a more prolonged sustained release with respect to the uncoated NGs considering the fact that amine and pyridine constituted an obstacle to drug diffusion. Indeed drug-polymer interaction between drug molecules and organic coatings are able to modify release rates. Between them, pyridine moieties improve the performance of PEG-PEI NGs in accordance with literature [58–60].

The influence of the system in delivering RhB was studied plotting release percentage against the time to the power of 0.43 ($t^{1/2.3}$ in Figure 6C). A linear plot is representative of Fickian diffusion and the y- axis intercept value is an indication of burst release, where it is well known that an ideal controlled release system should present linear trend during time and its y-axis intercept equal to zero. In neat NGs, RhB release showed a linear trend for the first 6 h, whereas for NG-am and NG-pyr it is extended until 12 hours underlining the efficacy of decorative strategies in improving release performances of the colloids. Another advantage is represented by the reduction of burst release, commonly known as one the unwanted phenomenon in drug delivery devices. This value is around 30% for NGs, 16% for NG-am and 4.2% for NG-pyr. Release data were used to estimate the RhB diffusion coefficients and the numeric value are presented in Table 3. The diffusion coefficients are calculated according to the theoretical approach described in Materials and Methods. In accordance with release studies, diffusivity for uncoated NGs presents higher values (one order of magnitude) compared to coated NGs. RhB is a bulky compound with a hydrophilic character [61]. Mesoscale calculations revealed that the functionalization with primary amines led to a more hydrophobic microenvironment within the outer layer compared to NG-ref (Figure 4A). This could make the partition of the drug inside the shell more favorable, correlating with the reduction in the diffusion coefficient. At the same time, NG-am is characterized by large (compared to RhB size) unfunctionalized areas. These leave free space for direct diffusion of the drug into the bulk solvent and might explain the similarity in release with NG-ref on long timescales.
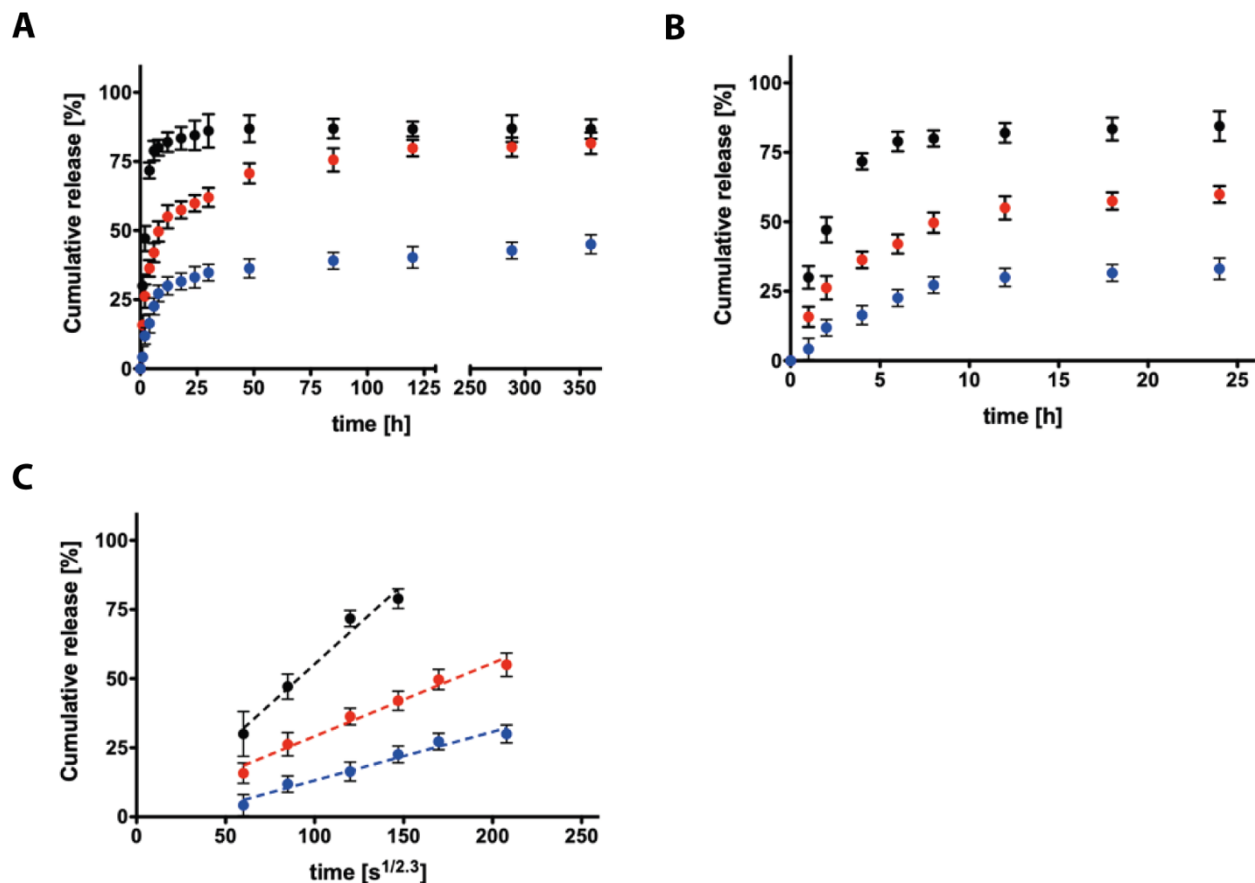
Figure 6. (A, B) In vitro release profile of RhB at pH = 7.4 from NG-ref (black circles), NG-am (red circles) and NG-pyr (blue circles) at different time scales. (C) The slope of RhB release at pH = 7.4 from neat NG-ref (black circles), NG-am (red circles) and NG-pyr (blue circles) against the variable time expressed as $t^{1/2.3}$ is representative of the Fickian diffusion coefficient of drugs in NGs ($p < 0.0001$ between all of the groups). The values are calculated as a percentage with respect to the total mass loaded (mean value ± standard deviation is plotted).

Table 3. Diffusion coefficients of RhB from NG-ref, NG-am and NG-pyr.

Nanogel type	$D_{RhB}{}^{a}$ [cm^2/s]
NG-ref	3.19
NG-am	1.02
NG-pyr	0.15

^{a} All values have to be multiplied for 10^{-5}.

NG-pyr is even less hydrated compared to NG-am (Figure 4C). At the same time, it is more crowded with respect to NG-am and this enhances the likelihood for RhB to come into contact with the pyridinic groups. Moreno-Villoslada et al. demonstrated the ability of RhB of establishing persistent π-π interactions with aromatic moieties present on water-soluble polymer matrices [62]. Therefore, diffusion may be further hindered by favorable molecular interactions taking place between RhB and the decoration layer. All these evidences are instructive in interpreting the considerably lower diffusion coefficient and delayed release observed for NG-pyr.

4. Conclusions

In this work we have proposed different decoration strategies on the same nanostructure core. The physical characterization of the final systems together with the drug release tests demonstrated that the presence of a different surface layer on the same nanostructure core determines on the whole system quantifiable differences in its behavior. Moreover, molecular modeling proofs the need of proper control and characterization of the functionalization as well as the role of the molecular features of the modified nanogel at the microscale.

References

[1]   P. Rameshkumar, R. Ramaraj, Gold nanoparticles deposited on amine functionalized silica sphere and its modified electrode for hydrogen peroxide sensing, J. Appl. Electrochem. 43 (2013) 1005–1010. https://doi.org/10.1007/s10800-013-0589-3.

[2]   K. McNamara, S.A.M. Tofail, Nanoparticles in biomedical applications, Adv. Phys. X. 2 (2017) 54–88. https://doi.org/10.1080/23746149.2016.1254570.

[3]   A.B. Chinen, C.M. Guan, J.R. Ferrer, S.N. Barnaby, T.J. Merkel, C.A. Mirkin, Nanoparticle Probes for the Detection of Cancer Biomarkers, Cells, and Tissues by Fluorescence, Chem. Rev. 115 (2015) 10530–10574. https://doi.org/10.1021/acs.chemrev.5b00321.

[4]   Y.K. Sung, S.W. Kim, Recent advances in the development of gene delivery systems, Biomater. Res. 23 (2019) 1–7. https://doi.org/10.1186/s40824-019-0156-z.

[5]   J. Chen, Z. Guo, H. Tian, X. Chen, Production and clinical development of nanoparticles for gene delivery, Mol. Ther. - Methods Clin. Dev. 3 (2016) 16023. https://doi.org/10.1038/mtm.2016.23.

[6]   N. Mishra, P. Pant, A. Porwal, J. Jaiswal, M. Aquib, Targeted Drug Delivery: A Review, Am. J. Pharm. Tech. Res. 6 (2016) 2249–3387.

[7]   W.J. Geldenhuys, M.T. Khayat, J. Yun, M.A. Nayeem, Drug Delivery and Nanoformulations for the Cardiovascular System., Res. Rev. Drug Deliv. 1 (2017) 32–40.

[8]   P. Dong, K.P. Rakesh, H.M. Manukumar, Y. Hussein, E. Mohammed, Innovative nano-carriers in anticancer drug delivery-a comprehensive review, Bioorg. Chem. 85 (2019) 325–336. https://doi.org/10.1016/j.bioorg.2019.01.019.

[9]   L. Yang, H. Mao, Y.A. Wang, Z. Cao, X. Peng, X. Wang, H. Duan, C. Ni, Q. Yuan, G. Adams, M.Q. Smith, W.C. Wood, X. Gao, S. Nie, Single Chain Epidermal Growth Factor Receptor Antibody Conjugated Nanoparticles for in vivo Tumor Targeting and Imaging, 98195 (2009) 235–243. https://doi.org/10.1002/smll.200800714.

[10]   C. Vissers, G. li Ming, H. Song, Nanoparticle technology and stem cell therapy team up

against neurodegenerative disorders, Adv. Drug Deliv. Rev. 148 (2019) 239–251. https://doi.org/10.1016/j.addr.2019.02.007.

[11]   S. Papa, F. Rossi, R. Ferrari, A. Mariani, M. De Paola, I. Caron, F. Fiordaliso, C. Bisighini, E. Sammali, C. Colombo, M. Gobbi, M. Canovi, J. Lucchetti, M. Peviani, M. Morbidelli, G. Forloni, G. Perale, D. Moscatelli, P. Veglianese, Selective nanovector mediated treatment of activated proinflammatory microglia/macrophages in spinal cord injury, ACS Nano. 7 (2013) 9881–9895. https://doi.org/10.1021/nn4036014.

[12]   H. Zhang, Y. Zhai, J. Wang, G. Zhai, New progress and prospects: The application of nanogel in drug delivery, Mater. Sci. Eng. C. 60 (2016) 560–568. https://doi.org/10.1016/j.msec.2015.11.041.

[13]   I. Neamtu, A.G. Rusu, A. Diaconu, L.E. Nita, A.P. Chiriac, Basic concepts and recent advances in nanogels as carriers for medical applications, Drug Deliv. 24 (2017) 539–557. https://doi.org/10.1080/10717544.2016.1276232.

[14]   M. Liu, H. Du, W. Zhang, G. Zhai, Internal stimuli-responsive nanocarriers for drug delivery: Design strategies and applications, Mater. Sci. Eng. C. 71 (2017) 1267–1280. https://doi.org/10.1016/j.msec.2016.11.030.

[15]   S. Hajebi, N. Rabiee, M. Bagherzadeh, S. Ahmadi, M. Rabiee, H. Roghani-Mamaqani, M. Tahriri, L. Tayebi, M.R. Hamblin, Stimulus-responsive polymeric nanogels as smart drug delivery systems, Acta Biomater. 92 (2019) 1–18. https://doi.org/10.1016/j.actbio.2019.05.018.

[16]   Z. Karami, M.R. Saghatchi Zanjani, M. Hamidi, Nanoemulsions in CNS drug delivery: recent developments, impacts and challenges, Drug Discov. Today. 24 (2019) 1104–1115. https://doi.org/10.1016/j.drudis.2019.03.021.

[17]   D.K. Ho, B.L.B. Nichols, K.J. Edgar, X. Murgia, B. Loretz, C.M. Lehr, Challenges and strategies in drug delivery systems for treatment of pulmonary infections, Eur. J. Pharm. Biopharm. 144 (2019) 110–124. https://doi.org/10.1016/j.ejpb.2019.09.002.

[18]   F. Pinelli, A. Sacchetti, G. Perale, F. Rossi, Is nanoparticle functionalization a versatile

approach to meet the challenges of drug and gene delivery?, Ther. Deliv. 11 (2020).

https://doi.org/10.4155/tde-2020-0030.

[19]   F. Pinelli, G. Perale, F. Rossi, Coating and functionalization strategies for nanogels and

nanoparticles for selective drug delivery, Gels. 6 (2020).

https://doi.org/10.3390/gels6010006.

[20]   D. Wang, L.P. Wu, Nanomaterials for delivery of nucleic acid to the central nervous system

(CNS), Mater. Sci. Eng. C. 70 (2017) 1039–1046.

https://doi.org/10.1016/j.msec.2016.04.011.

[21]   D.R. Hristov, L. Rocks, P.M. Kelly, S.S. Thomas, A.S. Pitek, P. Verderio, E. Mahon, K.A.

Dawson, Tuning of nanoparticle biological functionality through controlled surface

chemistry and characterisation at the bioconjugated nanoparticle surface, Sci. Rep. 5 (2015)

1–8. https://doi.org/10.1038/srep17040.

[22]   A.G. Kolhatkar, A.C. Jamison, D. Litvinov, R.C. Willson, T.R. Lee, Tuning the magnetic

properties of nanoparticles, 2013. https://doi.org/10.3390/ijms140815977.

[23]   N. Viriyakitpattana, P. Sunintaboon, Synthesis of crosslinked poly(methacrylic acid)

shell/lipid core colloidal nanoparticles via L-in-Lm interfacial polymerization and their pH

responsiveness, Colloids Surfaces A Physicochem. Eng. Asp. 603 (2020) 125180.

https://doi.org/10.1016/j.colsurfa.2020.125180.

[24]   X. Chen, C. Gao, Influences of size and surface coating of gold nanoparticles on

inflammatory activation of macrophages, Colloids Surfaces B Biointerfaces. 160 (2017)

372–380. https://doi.org/10.1016/j.colsurfb.2017.09.046.

[25]   L.A. Frank, G.R. Onzi, A.S. Morawski, A.R. Pohlmann, S.S. Guterres, R. V. Contri,

Chitosan as a coating material for nanoparticles intended for biomedical applications, React.

Funct. Polym. 147 (2020) 104459. https://doi.org/10.1016/j.reactfunctpolym.2019.104459.

[26]   N. Sahiner, Preparation of poly(ethylene imine) particles for versatile applications, Colloids

Surfaces A Physicochem. Eng. Asp. 433 (2013) 212–218.

https://doi.org/10.1016/j.colsurfa.2013.05.029.

[27]   G.T. Vladisavljević, Preparation of microemulsions and nanoemulsions by membrane

emulsification, Colloids Surfaces A Physicochem. Eng. Asp. 579 (2019).

https://doi.org/10.1016/j.colsurfa.2019.123709.

[28]   E. Mauri, P. Veglianese, S. Papa, A. Mariani, M. De Paola, R. Rigamonti, G.M.F.

Chincarini, S. Rimondo, A. Sacchetti, F. Rossi, Chemoselective functionalization of nanogels

for microglia treatment, Eur. Polym. J. 94 (2017) 143–151.

https://doi.org/10.1016/j.eurpolymj.2017.07.003.

[29]   E. Mauri, P. Veglianese, S. Papa, A. Rossetti, M. De Paola, A. Mariani, Z. Posel, P. Posocco,

A. Sacchetti, F. Rossi, Effects of primary amine-based coatings on microglia internalization

of nanogels, Colloids Surfaces B Biointerfaces. 185 (2020).

https://doi.org/10.1016/j.colsurfb.2019.110574.

[30]   I. Vismara, S. Papa, V. Veneruso, E. Mauri, A. Mariani, M. De Paola, R. Affatato, A.

Rossetti, M. Sponchioni, D. Moscatelli, A. Sacchetti, F. Rossi, G. Forloni, P. Veglianese,

Selective Modulation of A1 Astrocytes by Drug-Loaded Nano-Structured Gel in Spinal Cord

Injury, ACS Nano. 14 (2020) 360–371. https://doi.org/10.1021/acsnano.9b05579.

[31]   S. Vinogradov, E. Batrakova, A. Kabanov, Poly(ethylene glycol)-polyethyleneimine

NanoGel(TM) particles: Novel drug delivery systems for antisense oligonucleotides,

Colloids Surfaces B Biointerfaces. 16 (1999) 291–304. https://doi.org/10.1016/S0927-

7765(99)00080-6.

[32]   E. Mauri, F. Rossi, A. Sacchetti, Tunable drug delivery using chemoselective

functionalization of hydrogels, Mater. Sci. Eng. C. 61 (2016) 851–857.

https://doi.org/10.1016/j.msec.2016.01.022.

[33]   E. Mauri, F. Cappella, M. Masi, F. Rossi, PEGylation influences drug delivery from

nanogels, J. Drug Deliv. Sci. Technol. 46 (2018) 87–92.

https://doi.org/10.1016/j.jddst.2018.05.003.

[34] G. Perale, P. Arosio, D. Moscatelli, V. Barri, M. Müller, S. Maccagnan, M. Masi, A new model of resorbable device degradation and drug release: Transient 1-dimension diffusional model, J. Control. Release. 136 (2009) 196–205. https://doi.org/10.1016/j.jconrel.2009.02.014.

[35] A. Martín-Molina, M. Quesada-Pérez, A review of coarse-grained simulations of nanogel and microgel particles, J. Mol. Liq. 280 (2019) 374–381. https://doi.org/10.1016/j.molliq.2019.02.030.

[36] I. V. Volgin, S. V. Larin, A. V. Lyulin, S. V. Lyulin, Coarse-grained molecular-dynamics simulations of nanoparticle diffusion in polymer nanocomposites, Polymer (Guildf). 145 (2018) 80–87. https://doi.org/10.1016/j.polymer.2018.04.058.

[37] P. Posocco, C. Gentilini, S. Bidoggia, A. Pace, P. Franchi, M. Lucarini, M. Fermeglia, S. Pricl, L. Pasquato, Self-organization of mixtures of fluorocarbon and hydrocarbon amphiphilic thiolates on the surface of gold nanoparticles, ACS Nano. 6 (2012) 7243–7253. https://doi.org/10.1021/nn302366q.

[38] M. Șologan, D. Marson, S. Polizzi, P. Pengo, S. Boccardo, S. Pricl, P. Posocco, L. Pasquato, Patchy and Janus Nanoparticles by Self-Organization of Mixtures of Fluorinated and Hydrogenated Alkanethiolates on the Surface of a Gold Core, ACS Nano. 10 (2016) 9316–9325. https://doi.org/10.1021/acsnano.6b03931.

[39] Z. Posel, M. Svoboda, Z. Limpouchová, M. Lísal, K. Procházka, Adsorption of amphiphilic graft copolymers in solvents selective for the grafts on a lyophobic surface: A coarse-grained simulation study, Phys. Chem. Chem. Phys. 20 (2018) 6533–6547. https://doi.org/10.1039/c7cp08327k.

[40] Z. Posel, P. Posocco, M. Lísal, M. Fermeglia, S. Pricl, Highly grafted polystyrene/polyvinylpyridine polymer gold nanoparticles in a good solvent: Effects of chain length and composition, Soft Matter. 12 (2016) 3600–3611.

https://doi.org/10.1039/c5sm02867a.

[41] J. Cheng, A. Vishnyakov, A. V. Neimark, Morphological transformations in polymer brushes in binary mixtures: DPD study, Langmuir. 30 (2014) 12932–12940. https://doi.org/10.1021/la503520e.

[42] C.M. Hansen, Hansen Solubility Parameters: A User's Handbook, 2007.

[43] A. Khedr, A. Striolo, DPD Parameters Estimation for Simultaneously Simulating Water-Oil Interfaces and Aqueous Nonionic Surfactants, J. Chem. Theory Comput. 14 (2018) 6460–6471. https://doi.org/10.1021/acs.jctc.8b00476.

[44] X. Tang, W. Zou, P.H. Koenig, S.D. McConaughy, M.R. Weaver, D.M. Eike, M.J. Schmidt, R.G. Larson, Multiscale Modeling of the Effects of Salt and Perfume Raw Materials on the Rheological Properties of Commercial Threadlike Micellar Solutions, J. Phys. Chem. B. 121 (2017) 2468–2485. https://doi.org/10.1021/acs.jpcb.7b00257.

[45] C. Ibergay, P. Malfreyt, D.J. Tildesley, Electrostatic interactions in dissipative particle dynamics: Toward a mesoscale modeling of the polyelectrolyte brushes, J. Chem. Theory Comput. 5 (2009) 3245–3259. https://doi.org/10.1021/ct900296s.

[46] S. Plimpton, Fast parallel algorithms for short-range molecular dynamics, J. Comput. Phys. 117 (1995) 1–19. https://doi.org/10.1006/jcph.1995.1039.

[47] Y. Omidi, V. Kafil, Cytotoxic Impacts of Linear and Branched Polyethylenimine Nanostructures in A431 Cells, BioImpacts. 1 (2011) 23–30. http://bi.tbzmed.ac.ir/.

[48] I. Vismara, S. Papa, V. Veneruso, E. Mauri, A. Mariani, M. De Paola, R. Affatato, A. Rossetti, M. Sponchioni, D. Moscatelli, A. Sacchetti, F. Rossi, G. Forloni, P. Veglianese, Selective Modulation of A1 Astrocytes by Drug-Loaded Nano-Structured Gel in Spinal Cord Injury, ACS Nano. 14 (2020) 360–371. https://doi.org/10.1021/acsnano.9b05579.

[49] E. Mauri, I. Moroni, L. Magagnin, M. Masi, A. Sacchetti, F. Rossi, Comparison between two different click strategies to synthesize fluorescent nanogels for therapeutic applications, React. Funct. Polym. 105 (2016) 35–44.

https://doi.org/10.1016/j.reactfunctpolym.2016.05.007.

[50] F. Pinelli, F. Pizzetti, Ó. Fullana, A. Marchetti, A. Rossetti, A. Sacchetti, F. Rossi, Influence of the Core Formulation on Features and Drug Delivery Ability of Carbamate-Based Nanogels, Int. J. Mol. Sci. 21 (2020).

[51] Y. tae Kim, J.M. Caldwell, R. V. Bellamkonda, Nanoparticle-mediated local delivery of methylprednisolone after spinal cord injury, Biomaterials. 30 (2009) 2582–2590. https://doi.org/10.1016/j.biomaterials.2008.12.077.

[52] D.W. Brann, K. Dhandapani, C. Wakade, V.B. Mahesh, M.M. Khan, Neurotrophic and neuroprotective actions of estrogen: Basic mechanisms and clinical implications, Steroids. 72 (2007) 381–405. https://doi.org/10.1016/j.steroids.2007.02.003.

[53] C. Rodriguez-Tenreiro, C. Alvarez-Lorenzo, A. Rodriguez-Perez, A. Concheiro, J.J. Torres-Labandeira, Estradiol sustained release from high affinity cyclodextrin hydrogels, Eur. J. Pharm. Biopharm. 66 (2007) 55–62. https://doi.org/10.1016/j.ejpb.2006.09.003.

[54] J.L. Arias, F. Linares-Molinero, V. Gallardo, Á. V. Delgado, Study of carbonyl iron/poly(butylcyanoacrylate) (core/shell) particles as anticancer drug delivery systems. Loading and release properties, Eur. J. Pharm. Sci. 33 (2008) 252–261. https://doi.org/10.1016/j.ejps.2007.12.005.

[55] K. Ulbrich, K. Holá, V. Šubr, A. Bakandritsos, J. Tuček, R. Zbořil, Targeted Drug Delivery with Polymers and Magnetic Nanoparticles: Covalent and Noncovalent Approaches, Release Control, and Clinical Studies, Chem. Rev. 116 (2016) 5338–5431. https://doi.org/10.1021/acs.chemrev.5b00589.

[56] D. Ossipov, S. Kootala, Z. Yi, X. Yang, J. Hilborn, Orthogonal chemoselective assembly of hyaluronic acid networks and nanogels for drug delivery, Macromolecules. 46 (2013) 4105–4113. https://doi.org/10.1021/ma400543u.

[57] E. Mauri, G.M.F. Chincarini, R. Rigamonti, L. Magagnin, A. Sacchetti, F. Rossi, Modulation of electrostatic interactions to improve controlled drug delivery from nanogels, Mater. Sci.

Eng. C. 72 (2017) 308–315. https://doi.org/10.1016/j.msec.2016.11.081.

[58]   H. Chen, Y. Li, Y. Liu, T. Gong, L. Wang, S. Zhou, Highly pH-sensitive polyurethane exhibiting shape memory and drug release, Polym. Chem. 5 (2014) 5168–5174. https://doi.org/10.1039/c4py00474d.

[59]   Z. Geng, Y. Han, W. Jiang, Structural transformation of vesicles formed by a polystyrene-b-poly(acrylic acid)/polystyrene-b-poly(4-vinyl pyridine) mixture: from symmetric to asymmetric membranes, Soft Matter. 13 (2017) 2634–2642. https://doi.org/10.1039/C7SM00255F.

[60]   S. Rahim, S.A. Ali, F. Ahmed, M. Imran, M.R. Shah, M.I. Malik, Evaluation of morphology, aggregation pattern and size-dependent drug-loading efficiency of gold nanoparticles stabilised with poly (2-vinyl pyridine), J. Nanoparticle Res. 19 (2017). https://doi.org/10.1007/s11051-017-3933-4.

[61]   M. Adiraj Iyer, D.T. Eddington, Storing and releasing rhodamine as a model hydrophobic compound in polydimethylsiloxane microfluidic devices, Lab Chip. 19 (2019) 574–579. https://doi.org/10.1039/C9LC00039A.

[62]   I. Moreno-Villoslada, M. Jofré, V. Miranda, P. Chandía, R. González, S. Hess, B.L. Rivas, C. Elvira, J. San Román, T. Shibue, H. Nishide, π-Stacking of rhodamine B onto water-soluble polymers containing aromatic groups, Polymer (Guildf). 47 (2006) 6496–6500. https://doi.org/10.1016/j.polymer.2006.07.059.